

Space-Projected Conductivity and Spectral Properties of the Conduction Matrix

Kashi N. Subedi,* Kiran Prasai, and David A. Drabold

Herein, the Kubo–Greenwood formula is utilized to project the electronic conductivity into real space, and a Hermitian positive semidefinite matrix Γ is discussed, which is called the *conduction matrix*, that reduces the computation of spatial conduction activity to a diagonalization. It is shown that for low-density amorphous carbon, connected sp^2 rings and sp chains are conduction-active sites in the network. In amorphous silicon, transport involves hopping through tail states mediated by the defects near the Fermi level. It is found that for liquid silicon, thermal fluctuations induce spatial and temporal conductivity fluctuations in the material. The frequency-dependent absorption of light as a function of wavelength in an amorphous silicon suboxide (a-SiO_{1.3}) is also studied. It is shown that the absorption is strongly frequency dependent and selects out different oxygen vacancy subnetworks depending on the frequency. Γ is diagonalized to obtain conduction eigenvalues and eigenvectors, and it is shown that the density of states of the eigenvalues for FCC aluminum has an extended spectral tail that distinguishes metals from insulators and semiconductors. The method is easy to implement with any electronic structure code, providing suitable estimates for single-particle electronic states and energies.

formula (KGF). This was later generalized as the “Fluctuation-Dissipation theorem” that mathematically connects dissipative processes with equilibrium fluctuations.^[5] The ultimate roots of this work extend through time to Einstein and his work on Brownian motion and diffusion.^[6]

In this article, we briefly review our recently proposed method to estimate the spatially projected conductivity (SPC),^[7] apply it to a range of materials, and provide insights both into the materials we study and the method itself. The rest of this article is organized as follows. In Section 2, we review the KGF. In Section 3, we discuss background material on computing spatial transport information from computer models of materials. In Section 4, we describe our method, and in Section 5 we offer computational details and the models used. In Section 6, we explore five different systems: a low-density phase of amorphous carbon (a-C), amorphous and liquid silicon (l-Si), amorphous silicon (a-Si) suboxide,

and for a useful contrast, FCC aluminum. We draw conclusions in Section 7.

1. Introduction

Practical calculation of electron transport in materials^[1] always involves assumptions and approximations. The most natural and oldest approach is to use Boltzmann’s equation,^[2] which is ideal for a crystalline system with relatively weak impurity or thermal disorder. Implicit to such a picture is the assumption that \mathbf{k} is a good quantum number associated with the assumed lattice. A different way of framing the problem is due to Kubo,^[3] who in 1957 computed the linear response (current) to an external electric field. The resulting expression for the electrical conductivity, further approximated within a single-particle picture of the electronic structure,^[4] is called the Kubo–Greenwood

2. Kubo Formula

For calculations of charge transport in topologically disordered systems (amorphous or liquid), for which there is no underlying lattice, it is natural to adopt the Kubo approach. Mott and Davis^[8] and Moseley and Lukes^[9] offered an appealing physical derivation of the KGF that we tersely repeat here. Consider a system with an applied (external) AC electric field \mathbf{E} . The system absorbs photons from the electromagnetic field, and this drives electronic transitions near the Fermi level, ϵ_F . Associated with this field, there is an electric current density \mathbf{j} . The Joule heat produced by the electric field per unit time is $\Omega \mathbf{j} \cdot \mathbf{E}$, where Ω is the cell volume. The rate at which energy is absorbed from electronic transitions is $\gamma = \sum_{if} \epsilon_{fi} (w_{fi} P_i - w_{if} P_f)$. Here ϵ_{fi} is the energy difference between initial and final states, w_{fi} is the transition probability per unit time between final state f and initial state i , and $P_{i(f)}$ is the occupation probability of the initial (final) state. Next, one assumes that $\gamma = \Omega \mathbf{j} \cdot \mathbf{E}$. By using Fermi’s Golden Rule to estimate the transition probabilities, and defining the conductivity σ from the identification that $\sigma E^2/2$ is the mean rate of energy loss per unit volume, one obtains the KGF for each k -point \mathbf{k} ^[3,4] (written here in a form most convenient for our purposes)

K. N. Subedi, Prof. D. A. Drabold
Department of Physics and Astronomy
Ohio University
Athens, OH 45701, USA
E-mail: ks173214@ohio.edu, kashi.subedi@gmail.com

Dr. K. Prasai
E. L. Ginzton Lab
Stanford University
Stanford, CA 94305, USA

 The ORCID identification number(s) for the author(s) of this article can be found under <https://doi.org/10.1002/pssb.202000438>.

DOI: 10.1002/pssb.202000438

$$\sigma_{\mathbf{k}}(\omega) = \sum_{i,j} g_{ij}(\mathbf{k}, \omega) \sum_{\alpha} |p_{ij}^{\alpha}|^2 \quad (1)$$

In the shorthand notation of Equation (1), we averaged over diagonal elements of the conductivity tensor (α represents Cartesian directions), i and j index Kohn–Sham orbitals (or other single-particle states) $\psi_{i,\mathbf{k}}(x)$ with associated energies $\epsilon_{i,\mathbf{k}}$, p^{α} is the momentum operator (for direction α : $p^{\alpha} = -i\hbar\partial/\partial x_{\alpha}$) and $g_{ij}(\mathbf{k}, \omega) = 2\pi e^2 [f_i(\mathbf{k}) - f_j(\mathbf{k})] \delta(\epsilon_j(\mathbf{k}) - \epsilon_i(\mathbf{k}) - \hbar\omega) / (3m^2\omega\Omega)$, and f is the Fermi–Dirac distribution. The matrix elements of the momentum operator are $p_{ij}^{\alpha} = \langle \psi_j | p^{\alpha} | \psi_i \rangle$. This is devised for amorphous materials which are assumed to be isotropic; it is equally easy to implement this method for a particular direction to explore anisotropy of conduction. It is remarkable that this expression for the conductivity, which exactly coincides with the study by Greenwood,^[4] does not require an explicit expression for the current density. By carefully deriving the current density \mathbf{j} , one discovers that this derivation, and also Greenwood’s, veils significant approximations involving the DC limit, and more subtly, the spatial homogeneity of carrier density. We will not further dwell on these technical issues here, and adopt the “standard” KGF (Equation (1)). See, for example, Equation 19 in the study by Zhang and Drabold^[10] and associated discussion. For a full many-body picture, see the previous studies by Zhang and Drabold.^[11,12]

The Kubo formula has been heavily used in liquids,^[13–16] amorphous semiconductors,^[17] and mixed systems.^[18,19] In its usual application, the KGF is applied to a static disordered lattice. As such, it provides no information about thermal disorder and its consequences to conduction. For applications of the KGF in disordered systems, the electron–phonon coupling is large for localized single-particle states,^[20,21] especially those orbitals near the Fermi energy. In a room temperature thermal molecular dynamics simulation, energy levels may fluctuate with a thermally induced root mean squared fluctuation $\sigma_E \gg kT$.^[22,23]

Above the Debye temperature, it is sensible to estimate the temperature-dependent conductivity by undertaking a long constant-temperature molecular dynamics (MD) simulation and averaging the KGF over the trajectory. This seems to give reasonable results for the temperature dependence of pure and hydrogenated a-Si, and explains the high-temperature coefficient of resistance and functionality of doped a-Si:H as a material for night-vision device applications.^[24]

Apart from the approximations mentioned earlier, there are many technical details for properly using the KGF, including finite size effects and such details as the broadening of the δ function in Equation (1). A recent review details many issues about the use of KGF in hot condensed matter.^[25] The KGF is a valuable tool, linking as it does transport experiments to the quantum mechanics of materials, but in its usual implementation gives just one function (the AC conductivity) or one *number* (the DC conductivity). It provides no spatial information about the conduction.

3. Computing Spatial Information about Transport

For heterogeneous systems, a basic question is: “what parts of the network are conducting?” Some emerging computer memory technologies (resistive random access memory [RAM] and

conducting bridge RAM) involve specific conduction pathways, and our microscopic understanding of such systems might be improved by a detailed atomistic understanding of the flow of charge through the systems. Conducting bridge RAM can be made from many amorphous insulating hosts (such as GeSe₃ or Al₂O₃, heavily doped with a transition metal like Ag or Cu). These are technologically important electrochemical devices for which basic questions arise about whether transport is simply through metal filaments or a more intricate process involving transport through metal-rich regions.^[26] We have provided insight into this elsewhere.^[7,26–29] Another example of keen current interest is physical unclonable function (PUF) devices for computer security, made from a-Si suboxide materials, as we discuss on more detail in Section 6.4. Another example of interest is conductance fluctuation in amorphous systems.^[30]

With this tool in hand, the idea might also be pushed in an engineering direction as a common inverse problem of materials science: “what is the structure that I need to have a particular conductivity?”, or “what is the structure required to have a particular absorption of light of frequency ω , eg., for the design of waveguides?” The inverse problem is always challenging: a robust tool of the form $\mathbf{R} \rightarrow \wp$ (given coordinates what is the conducting path) is required before we can handle $\wp \rightarrow \mathbf{R}$ (given the conducting path we seek, what coordinates—structure—will yield it?).

Some existing schemes yield insight into the spatial character of conduction. A principal message of the KGF is that the DC conductivity arises from transitions between states at or near the Fermi level. To obtain a nonzero conductivity, it is necessary that the momentum matrix element not vanish between the relevant occupied and unoccupied states (Equation (1)). If two such states ψ_i and ψ_j do not overlap, there is no contribution to the conductivity: transitions between spatially nonoverlapping orbitals are forbidden. So, to the extent that there is a large overlap between the two states, there is likely to be a larger momentum matrix element too. This is the idea behind a primitive approximation, the “ $q_i - q_j$ ” method that we use in ref. [27]. An even simpler scheme is to compute the charge density around the Fermi level^[31]—it must be that the spatial conductivity involves those parts of space where this charge density is large, but this totally ignores the momentum matrix elements which lie at the heart of the KGF—these matrix elements are a legacy of the current–current correlation function, and it is not desirable to neglect these contributions. Other ideas related to spatial decomposition of conductivity have emerged in the literature before, including a computation of current densities for a randomly disordered system,^[32] using the methods of Baranger and Stone.^[33] Also, within a Landauer picture, the concept of transmission eigen-channels was introduced and later implemented with non-equilibrium Green’s functions.^[34]

4. Theory

4.1. SPC

The KGF (Equation (1)) gives the conductivity as a weighted sum of the modulus squared momentum matrix elements. The sums on Latin indices are over single-particle, for this article, Kohn–

Sham orbitals. The spatial dependence of the states is obviously important, but only insofar as this modulates the momentum matrix elements. Thus, it is desirable to rewrite the KGF expressing the matrix element quadratures as sums on a real space grid to find a spatial decomposition. Suppressing the explicit dependence of σ on \mathbf{k} and ω , we write

$$\sigma = \sum_{ij\alpha} \int d^3x \int d^3x' g_{ij} [\psi_i^*(x) p^\alpha \psi_j(x)] [\psi_i^*(x') p^\alpha \psi_j(x')]^* \quad (2)$$

Next, define complex-valued functions

$$\xi_{ij}^\alpha(x) = \psi_i^*(x) p^\alpha \psi_j(x) \quad (3)$$

on a discrete real-space grid (call the grid points x), and suppose, for simplicity, that the grid is uniformly spaced in 3D space with spacing h . Approximating the integrals as sums on the grid, and obtaining the operation of p^α from centered finite differences, we easily arrive at

$$\sigma \approx h^6 \sum_{x, x'} \sum_{ij\alpha} g_{ij} \xi_{ij}^\alpha(x) [\xi_{ij}^\alpha(x')]^* \quad (4)$$

We find it useful to introduce what we will call the *conduction matrix* Γ defined as

$$\Gamma(x, x') = h^6 \sum_{ij\alpha} g_{ij} \xi_{ij}^\alpha(x) [\xi_{ij}^\alpha(x')]^* \quad (5)$$

Γ is Hermitian and positive semidefinite. Note that Γ has the dimension of conductivity, and we have summed out the Kohn–Sham orbitals, leaving only spatial dependence. It follows from Equation (4) that $\sigma = \sum_{x, x'} \Gamma(x, x')$ as $h \rightarrow 0$. We take the SPC to be $\zeta(x) = |\sum_{x'} \Gamma(x, x')|$. To obtain a real value for the scalar field ζ , the modulus operation is required: while the full double sum is, of course, real, summing only one index of Γ yields a function that is, in general, complex. $\zeta(x)$ is of interest as it is positive, and by construction indicates the conduction-active parts of the system. Similar forms are possible for the SPC. If, for example, only one of the matrix elements is computed on a grid, then if $\phi_{ij} = h^3 g_{ij} p_{ij}^\alpha$, then for $\tau(x) = \sum_{ij\alpha} \phi_{ij} \xi_{ij}^\alpha(x)$, $|\tau|$ also serves as an estimate for SPC, identical to ζ as $h \rightarrow 0$.

4.2. Spectral Properties of the Conduction Matrix

The eigenvalue problem for Γ reads: $\Gamma|\chi_\mu\rangle = \Lambda_\mu|\chi_\mu\rangle$, for which $\mu = 1, n_g$. n_g is the number of points in the spatial grid (thus, for example, $n_g = n^3$ for n points in each Cartesian direction in 3D). Diagonalization provides a spectral representation: $\hat{\Gamma} = \sum_\mu |\chi_\mu\rangle \Lambda_\mu \langle \chi_\mu|$, from which

$$\sigma = \sum_\mu \Lambda_\mu [1 + \sum_{x, x', x \neq x'} \chi_\mu(x) \chi_\mu^*(x')] \quad (6)$$

Equation (6) introduces the concept of conduction eigenvalues and modes. The spectral decomposition of σ of Equation (6) categorizes the conductivity into a finite and, in practice, small (compared with the dimension of Γ) set of conduction channels. Because of trace invariance of Γ , $\sum_\mu \Lambda_\mu = \sum_x \Delta(x)$, for $\Delta(x) = \Gamma(x, x)$. The spectral form for the SPC is thus

$$\zeta_s(x) = \left| \sum_\mu \Lambda_\mu \{ |\chi_\mu(x)|^2 + \sum_{x', x' \neq x} \chi_\mu(x) \chi_\mu^*(x') \} \right| \quad (7)$$

and $\zeta(x) = \zeta_s(x)$. We observe that if we take a diagonal approximation $\Delta(x)$, by omitting the second term on the RHS in Equation (6), the eigenvalue Λ_μ would exactly give the conductance through channel μ . In such an approximation, $\sigma \sim \sum_\mu \Lambda_\mu = \text{Tr}(\Gamma)$, a form reminiscent of the transmission eigen-channels,^[34] but note that our full expression for σ is *not just a trace* over Γ in contrast with the transmission matrix appearing in the Landauer expression for conductance.

It is of interest to determine the value of an approximate ζ_s (e.g., computed from only a handful of the eigenvectors conjugate to the largest eigenvalues) to ζ . We discuss the density of states (DOS) of Γ later. For complex mixed conducting/insulating phases, we find that the eigenvectors χ conjugate to extremal eigenvalues produce a remarkably compact and efficient description of the conduction, often reproducing the full ζ with only a few tens of eigenvectors, even though $\text{dim}(\Gamma)$ is in the tens of thousands. For a metal (e.g., FCC Al), we again find a great accumulation of eigenvalues at $\Lambda = 0$ but with a significant spectral tail unseen in less metallic systems. Thus, the high conductivity of a metal accrues from integrating over this tail. The DOS of Γ is yet another way to distinguish insulators, semiconductors, and metals.

So far, we have computed the eigenvectors of Γ by exact diagonalization. However, it is clear that this problem is ideal for a Lanczos technique.^[35] A maximum entropy reconstruction of the DOS of Γ is also under investigation.^[36]

5. Computational Details

5.1. Models

In this article, we used Vienna Ab initio Simulation Package (VASP)^[37] code to carry out DFT calculations. The generalized gradient approximation (GGA) of Perdew–Burke–Ernzerhof (PBE)^[38] was used as the exchange–correlation functional. Brillouin zone sampling was restricted to the gamma point ($\mathbf{k} = 0$), and periodic boundary conditions were used throughout.

A model of low-density a-C was examined with density 1.5 g cm^{-3} and consisted of 216 atoms.^[39]

An a-Si model with 216 atoms ($\rho = 2.33 \text{ g cm}^{-3}$) was taken from the study by Djordjević et al.^[40] and was relaxed using a conjugate gradient method. While relatively small by current standards, this model is an excellent representation of the topology of a-Si, and is 100% fourfold, though some of the sites are strained. The a-Si model was then melted at 2000 K for 6 ps to create representative snapshots for l-Si.

We modeled a-Si suboxide (a-SiO_{1.3}) in cells with 184 atoms and density 1.68 g cm^{-3} ^[41] that was obtained using a melt-quench scheme.^[42] We began with a supercell with a random initial configuration at the experimental density and desired stoichiometry, which was then heated above melting point. The supercell was then cooled to room temperature in successive steps. The final model was obtained by performing a relaxation to minimize the forces acting on each atom to below $\approx 0.005 \text{ eV \AA}^{-1}$.

A cubic model of crystalline FCC Al (c-Al) with 500 atoms was constructed.

We use various values of grid spacing (h) throughout this article. We find that the SPC is fairly insensitive to h , and has checked the results presented here by considering a few different choices for h and verifying that the predicted SPCs were consistent.

5.2. Methods

To carry out the calculations, we used Kohn–Sham orbitals computed with VASP.^[43] The ξ (of Equation (4)) was obtained using finite central differences with $\delta r = 0.05 \text{ \AA}$. To estimate the SPC (ζ), we adopted a discrete grid with variable dimensions depending upon the supercell used. We selected a temperature of $T = 1000 \text{ K}$ for the Fermi–Dirac distribution and approximated the delta function in g_{ij} by a Gaussian with width 0.05 eV . The numerical value of the conductivity is sensitive to these choices, the SPC plots far less so.

The extent of the localization of eigenvectors was quantitatively gauged by calculating the inverse participation ratio (IPR) defined as

$$\mathcal{F}_\mu = \frac{\sum_x (\chi_\mu(x))^4}{(\sum_x (\chi_\mu(x))^2)^2} \quad (8)$$

The value of \mathcal{F} lies between 0 and 1. Higher \mathcal{F}_μ signifies that the eigenvector χ_μ is more spatially localized.

6. Results and Discussion

6.1. Low-Density a-C

Carbon materials have produced two Nobel prizes in the last quarter century. a-C has applications including protective coatings, radiation protection, electronic circuits, and biomedicine.^[44–46] Carbon-based electronics is a major field of research in materials science.^[47–50] Carbon in different forms

such as carbon nano tubes (CNTs) is being studied for PUF applications.^[51] Carbon-based electrodes are used as electrochemical sensors for biological applications.^[52]

a-C at low densities ($< 2 \text{ g cm}^{-3}$) consists primarily of sp^2 sites, with some sp and sp^3 sites. Bhattarai *et al.* have shown that a-C at low densities ($\rho = 0.92\text{--}1.6 \text{ g cm}^{-3}$) exhibits sp^2 configurations with $\approx 66\text{--}81\%$, sp chains with $\approx 14\text{--}33\%$, and sp^3 configurations with $\approx 0\text{--}9\%$.^[39] The presence of sp^2 and sp configurations may render the materials electrically conductive and optically absorbing. Intuitively, it is clear that the connectivity between the sp , sp^2 , and sp^3 subnetworks might also play a role in conduction. For densities below 1 g cm^{-3} , it has been shown that the material consists of warped and wrapped regions of amorphous graphene, with considerable ring disorder.^[53]

In this subsection, we discuss SPC in low-density a-C (1.5 g cm^{-3}) and also provide spectral information from the conduction matrix by diagonalizing it. We discretized the supercell into $40 \times 40 \times 40$ grid points ($h = 0.355 \text{ \AA}$) and obtained the conduction matrix $\Gamma(x, x')$ which has dimension of 64 000. The conductivity path was obtained by calculating space-projected conductivity at each grid point as discussed in earlier section (Section 4.1). The SPC is projected as an isosurface (yellow blob) in left plot of Figure 1. As a technical exercise, we also compare the results to the diagonal approximation $\Delta(x)$.

The isosurface in the left plot shows that SPC is due to both sp and sp^2 configurations in the network. It reveals active participation of sp chains in the network that form a clear connected conducting path and follow sp^2 configurations to a pentagonal ring. Pentagonal and the hexagonal ring structures that are connected with sp chains form the other active sites for conduction. These rings are highlighted in the middle plot of Figure 1 that show only those atoms contributing significantly to conduction. The arrows indicate the continuous conduction path along the C atoms displayed in the left plot. sp^3 configurations do not appear as SPC sites. As a consequence, they do not contribute to charge transport, as expected. To provide a simpler picture of the conduction, we projected $\Delta(x)$, the diagonal approximation of ζ , as an isosurface in the right plot of Figure 1. Δ is primarily centered on the

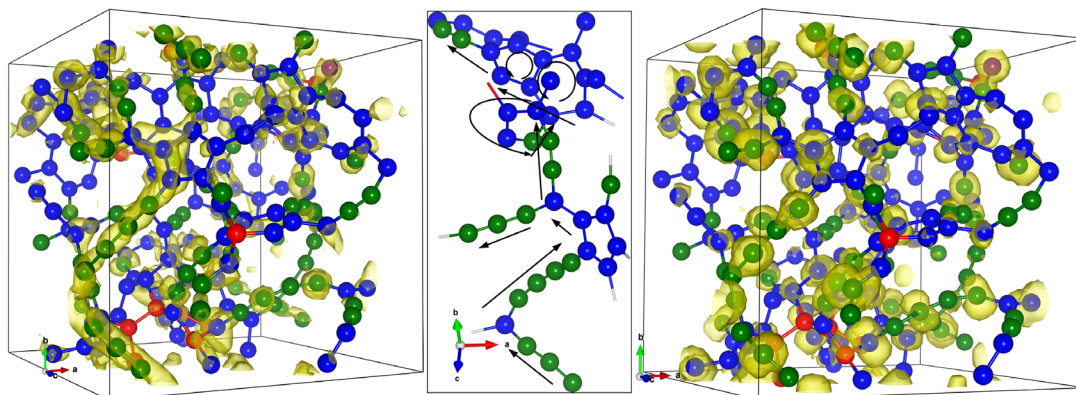


Figure 1. a-C: Left and right images correspond to the SPC (ζ) and the diagonal approximation $\Delta(x)$ projected on grids as an isosurface plot (yellow blobs), respectively. The middle plot corresponds to the structural topology of the network in one region of the supercell that forms a continuous conduction path. The straight and the curved lines with arrowhead are guides to the eye to indicate the conduction path. The colored spheres represent C atoms with different configurations; red (sp^3), blue (sp^2), green (sp), and purple (singly bonded).

atomic sites and shows discrete path. The isosurface blobs show that Δ picks almost the same sites that are active in ζ . So, Δ qualitatively provides a similar picture of the conduction path as ζ shown in left plot of Figure 1 for a-C.

Next, we discuss the spectral properties of conduction matrix, $\Gamma(x, x')$, for a-C by diagonalizing it as discussed earlier (Section 4.2). The DOS from the eigenvalues and the extent of the localization of the eigenvectors measured by IPR (\mathcal{I}) were calculated and are shown in **Figure 2**.

The DOS in Figure 2 reveals an overwhelming fraction of eigenvalues very near $\Lambda = 0$. These states are mostly localized as represented by the values of \mathcal{I} shown by the scattered red dots. We find a few eigenvalues significantly shifted from $\Lambda = 0$ in the spectrum; only eigenvectors corresponding to these extreme eigenvalues are important to the DC conductivity. To better estimate the number of such eigenvectors, we calculated the spectral form of SPC, (ζ_s), defined in Equation (7), from the

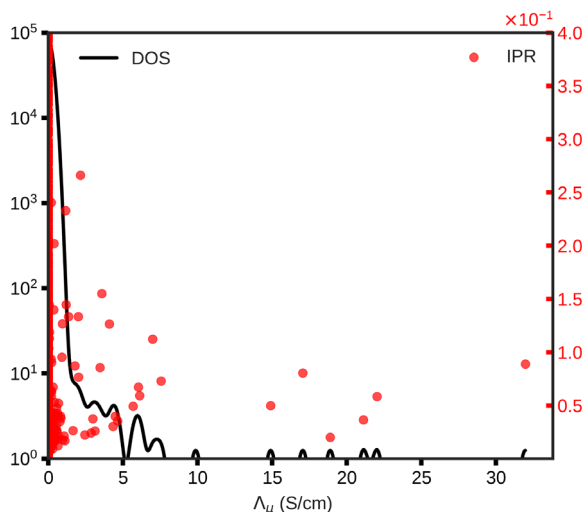


Figure 2. a-C: Logarithmic spectral DOS of Γ matrix. The left scale represents the DOS of the eigenvalues displayed in a log scale (solid black line) and the right scale corresponds to the extent of localization of eigenvectors measured as IPR (\mathcal{I}) (red circles). Large \mathcal{I} implies a spatially localized eigenvector of Γ .

largest 75 and 100 eigenvectors, and these are shown in **Figure 3**. Both isosurface plots in Figure 3 show almost the same path as ζ that is displayed in the left plot of Figure 1. This shows that 75–100 eigenvectors suffice to obtain the conduction path in a-C.

To see how two eigenvectors conjugate to the largest eigenvalues contribute to transport, see **Figure 4**. We see that from $\Lambda_\mu |\chi_\mu|^2$, these extremal eigenvectors either form a short channel or lie within spatially separated parts of the network. The eigenvector corresponding to the second largest eigenvalue (left plot in Figure 4) picks out mostly the sp sites. The sp^2 configurations which are adjacent to the sp configurations are other active sites for this eigenvalue. The extremal eigenvector selects both sp^2 and sp sites. Both eigenvectors pick more or less the same sp^2 sites in the network that are the active sites for the conduction as shown by ζ shown in left plot of Figure 1.

The physical conclusion is that sp chains play an important role in electronic transport in phases of carbon that possess them. The SPC that emerges reveals charge transport through interconnected sp chains and sp^2 rings. It is expected that the relative fraction of these conducting constituents is strongly density, impurity, and sample preparation dependent.

6.2. a-Si

a-Si plays an important role in technological applications, such as thin-film transistors, photovoltaics, infrared imaging devices, and active-matrix displays.^[54] Being an electronic material, understanding the conduction mechanisms is of obvious importance. In this subsection, we discuss the conduction-active sites in the material and also discuss the spectral properties of the conduction matrix Γ . The supercell was partitioned into $42 \times 42 \times 42$ grid points ($h = 0.39 \text{ \AA}$) and the Γ matrix was obtained. The SPC at each grid was then calculated and is shown as a heat map plot in **Figure 5**.

Earlier works on the electronic bandtails (Urbach tails) of a-Si have shown that the valence tail states are built from chains or clusters of Si atoms with bonds shorter than average and conduction tail states are due to chains of Si atoms with longer bonds.^[55–58] It is therefore to be expected that these tail states (and gap states due to badly strained fourfold sites or coordination defects) will play a role in conduction.

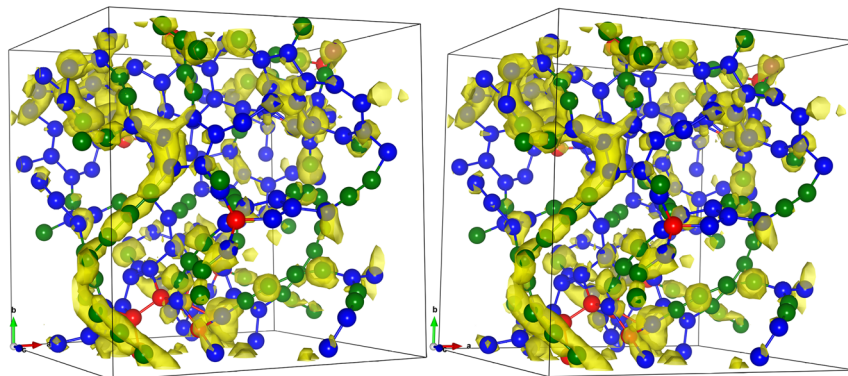


Figure 3. a-C: Spectral form for SPC (ζ_s) projected on grids as an isosurface plot (yellow blobs). Left and right plots correspond to the ζ_s from the sum of last 75 and 100 eigenvectors, respectively. Same cutoff for the isosurface has been used in both plots and the left plot in Fig. 1. Same color code is used to describe atoms as in Fig. 1. ζ_s from extreme 75–100 eigenvectors is equivalent to ζ and is sufficient to essentially exactly determine the SPC in a-C.

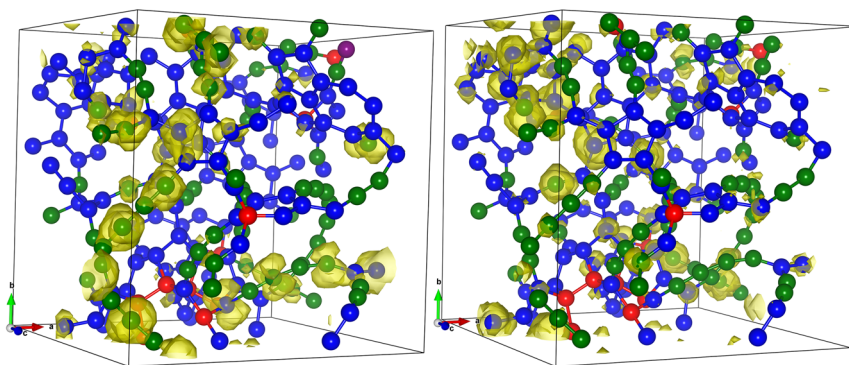


Figure 4. a-C: Eigenvectors projected on grids as an isosurface plot (yellow blobs). Left and right plots correspond to the second largest ($\Lambda_\mu = 22.04 \text{ S cm}^{-1}$) and the largest ($\Lambda_\mu = 31.98 \text{ S cm}^{-1}$) eigenvalues, respectively (refer to Figure 2). Same color code is used to describe atoms as in Figure 1.

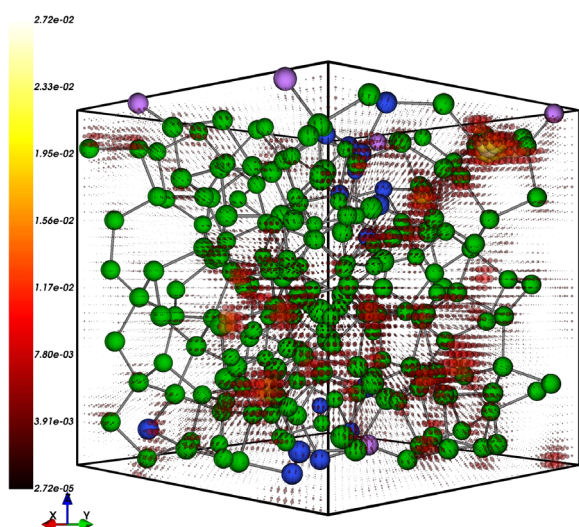


Figure 5. a-Si: SPC (ζ) projected on grids as heat map plot (labeled by colorbars on left of the plot) scaled with maximum value in each plot. The size of the hot spheres is scaled with the magnitude of the SPC value. The colored spheres represent Si atoms with different bonding environment; the blue and heliotrope colored spheres represent fourfold coordinated Si atoms with one and two very long Si–Si bonds, respectively. The green colored spheres represent typical Si atoms with normal bond lengths. The bond cutoff distance of 2.72 Å was chosen.

Figure 5 shows the SPC for a-Si. Analysis of the SPC shows special weight for atoms with bonds shorter than 2.32 Å and longer than 2.43 Å (the average bond length is about 2.35 Å). The heat map shows that the SPC also sits at strain defects (fourfold atoms with large variation in bond angles or bond lengths from tetrahedral symmetry). The conduction involves all the states near the Fermi level (ϵ_F), thus involving tail states (of long and short bond structures) and, of course, defect states near ϵ_F . We diagonalized Γ to understand the spectral information of the conduction eigenvalues and the eigenvectors. The DOS of the eigenvalues and the extent of localization (\mathcal{L}) of the eigenvectors were calculated and are shown in Figure 6.

Figure 6 shows a very large accumulation of eigenvalues near $\Lambda = 0$. Much about the transport can be obtained from only a few extremal eigenvalues and conjugate eigenvectors of Γ to

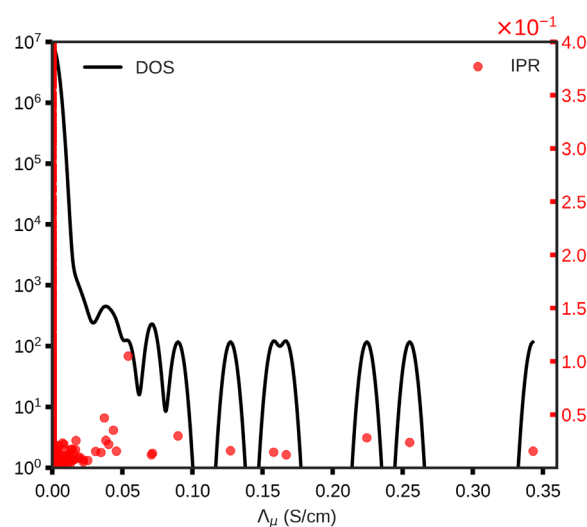


Figure 6. a-Si: Logarithmic spectral DOS of Γ matrix. The left scale corresponds to DOS of the eigenvalues displayed in a log scale (solid black line) and the right scale corresponds to the extent of localization measured as IPR (\mathcal{L}) (red circles).

approximate the SPC of the material. We plot $|\chi|^2$ for the largest two eigenvalues in Figure 7. We find that these eigenvectors select out specific sites in the network. The eigenvector corresponding to the second largest eigenvalue (left plot in Figure 7) picks the atomic sites with short-bonded Si atoms with maximum bond length of 2.32 Å. The eigenvector corresponding to the largest eigenvalue picks entirely different parts of the network. This eigenvector follows a path among those atoms that form adjacent strain defect sites,^[59] nominally fourfold but with one or two long bonds shown in blue and heliotrope, respectively, and also involves filaments of long Si–Si bonds with minimum bond length of 2.43 Å. This calculation reinforces the predicted short-bond (long-bond) association with valence (conduction) tails, and shows an interesting conduction mixing of the defects and tail structures (long- and short-bond subnetworks). In a system with dangling (threefold) or floating (fivefold) configurations, yielding states near ϵ_F , we would expect these sites to also participate in the resulting $\zeta(x)$.

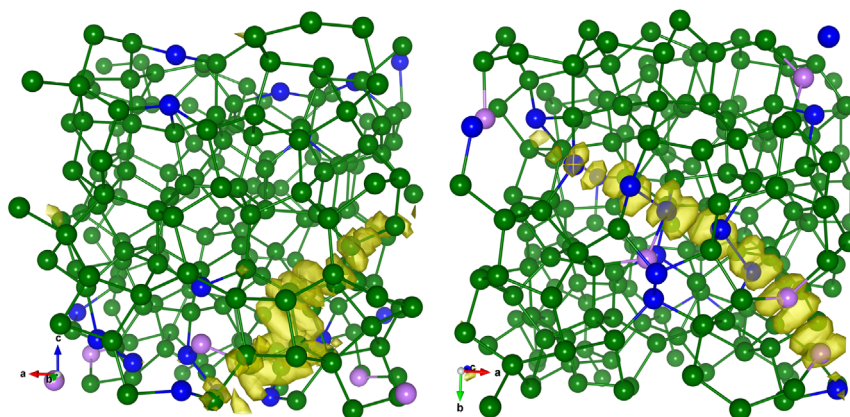


Figure 7. a-Si: Eigenvectors projected on grids as an isosurface plot (yellow blobs). Left and right plots correspond to the second largest ($\Lambda_{\mu} = 0.26 \text{ S cm}^{-1}$) and the largest ($\Lambda_{\mu} = 0.34 \text{ S cm}^{-1}$) eigenvalues, respectively. For atoms, the color code is same as used in Figure 5. As the atoms picked by the eigenvectors that are adjacent to each other are separated by the periodic box, we shifted the coordinates to make these atoms include in the same side of the box to make the connectivity clear. The left panel emphasizes short bonds, right panel long bonds, and defects.

In future work, we will explore defect-rich phases of amorphous Si including dangling and floating bonds (as well as nominally fourfold structures with strain defects) and explore the role of defects in conduction. There is no doubt that such defects will play a role, as their electronic energies are well known to be in the gap, and for dangling bonds especially, near the middle of the gap. We speculate that there may be interesting SPC linkages between such defects and the filamentary structures associated with the Urbach tails,^[56] perhaps reminiscent of the *sp*-ring mixing of a-C. Conductivity will certainly depend on delocalization that accrues from mixing/banding between defect state: such effects are included in our computations.

6.3. Conductivity Fluctuations in l-Si

l-Si is a metal in contrast to a-Si or c-Si which is tetrahedral semiconductors. Although it is metallic, the first neighbor atomic coordination number is between 5 and 6,^[60] hinting at a prevalence of covalent bonds in the liquid state of Si and differentiating it from other metals in terms of structural topology.^[61] In the liquid state, thermal fluctuations cause the structure to continuously change and so too the SPC in the network. To model the liquid metal, we annealed the a-Si model at 2000 K for 6 ps.

The thermal fluctuations induce fluctuations in the Fermi level (ϵ_F) and also the electronic gap associated with it. The fluctuation of the frontier of highest occupied molecular orbital (HOMO), lowest unoccupied molecular orbital (LUMO), and the Fermi level with simulation time is shown in **Figure 8** for a brief time interval.

From Figure 8, we see that the minute gamma-point gap opens and closes with time due to the thermal fluctuations. We chose four configurations as shown by different markers in the inset plot of Figure 8 where such feature exists. For these snapshots, we find that the coordination environment does not drastically change within the network for this short time interval. A majority of the Si atoms are fivefold and sixfold coordinated (≈ 56 – 57%); fourfold and sevenfold coordinated Si atoms account

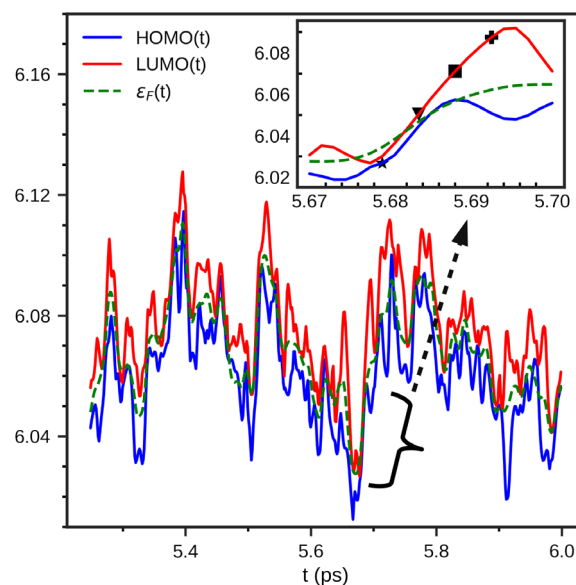


Figure 8. l-Si: A snapshot showing fluctuations of energy levels near the Fermi level (in eV) plotted against simulation time. The inset plot shows a specific region (shown by the curly brace) with closing and opening of the electronic gap. The markers correspond to the time step for the atomic configurations that were selected for the SPC calculations.

for ≈ 33 – 35% of the total coordination; and eightfold coordinated Si atoms account for 5.1–9.7% of the network. For each of these configurations, we obtained the SPC on a $40 \times 40 \times 40$ grids ($h = 0.41 \text{ \AA}$) and these are shown as heat map plots in **Figure 9**.

The heat map plot of SPC shows that the fluctuation in the energy levels results in slight variation in the SPC. For all models, we find that the SPC is quite extended, indicating the metallic character of the material. All coordinations seem involved in the conduction, suggesting a truly delocalized metallic form of conduction.

We also picked four temporally well-separated snapshots at simulation times 1.95, 3.15, 4.35, and 5.55 ps to capture the

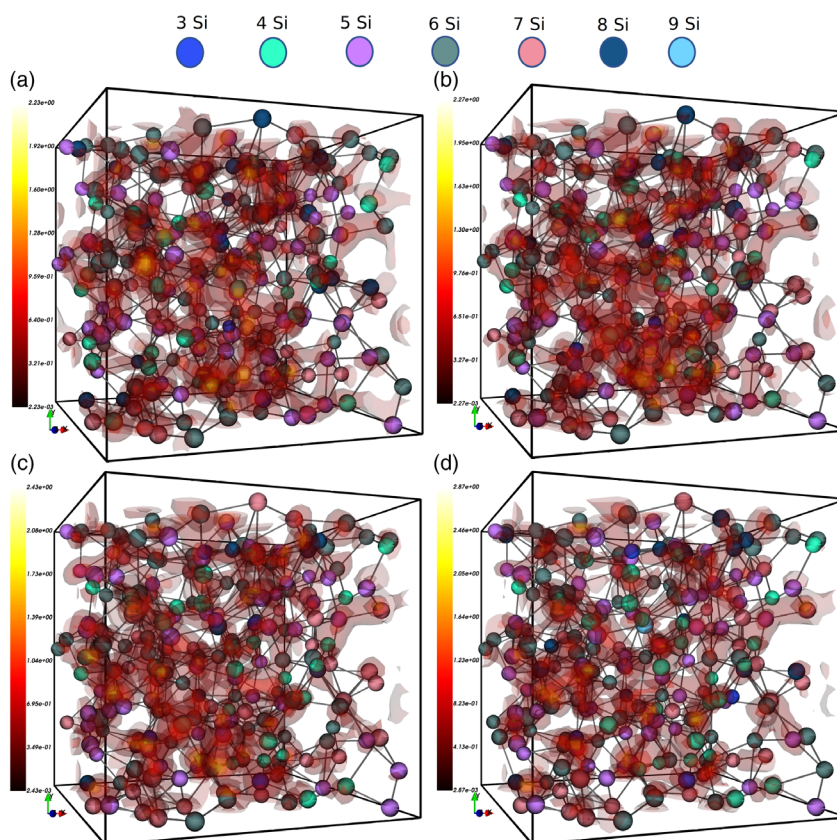


Figure 9. l-Si: SPC (ζ) projected on grids as a heat map (labeled by colorbars on left of each subplots) for atomic configurations at that are temporally close to each other shown by the marker signs in the inset plot of Figure 8. a–d) The atomic configurations shown by star, triangle, square, and the plus signs in the inset plots of Figure 8, respectively. Atom color represents Si with different instantaneous coordination as labeled and shown at the top of the figure. The cutoff distance of 3.10 Å is used to define the coordination.

variation of the conduction path on longer time scales. The SPC for each of these snapshots is shown on grids as a heat map in **Figure 10**. The dominating regions appear in different parts of the cell for these snapshots, an expected kind of “local conductance fluctuation” as the Si atoms diffuse in the liquid state and continuously change their local bonding and thus local electronic structure. The variation in the conduction path is displayed, and colored spheres in each plot of Figure 10 indicate the fluctuation in the local atomic environments. We find that, within the top 6% of SPC values in Figure 10a, one of the conduction paths is along the chain with fourfold, fivefold, sixfold, sevenfold coordinated Si atoms in the middle region of the network. Similarly, in Figure 10b, we find a continuous path along fourfold, fivefold, sixfold, sevenfold, eightfold Si atoms where four of such sixfold coordinated atoms contributing to the path. In Figure 10c, there exists a conduction path along a chain of five Si atoms that are all sixfold coordinated. We also find the conduction path along the chain of fourfold, fivefold, sixfold coordinated Si atoms where three of such fivefold coordinated Si exist in the chain. In Figure 10d, we find one of the conduction paths along six Si atoms with fivefold, sixfold, sevenfold, eightfold coordinated Si atoms forming a chain where three of them are fivefold coordinated. So, the SPC calculations from these snapshots show that the most conduction-active sites in l-Si are fivefold and sixfold

coordinated. We find Si atoms with fourfold, sevenfold, and eightfold coordinated forming the other sites of conduction. It would be of interest to properly analyze these fluctuations with suitable space-time correlation functions.

6.4. a-Si Suboxide: Application for Finite ω

Optical materials are critically important, and there is always a demand for novel optically functional and transparent materials. Electromagnetic waves of different frequencies may be absorbed by different parts of the inhomogeneous material. Having *a priori* information on the absorption-active sites/regions in the material could be helpful to engineers, for example, to design waveguides or other optical devices. Optical PUFs are an ongoing research topic for computer security applications.^[62]

Silicon suboxides, a-SiO_x (0 < x < 2), have complex structures and two different pictures of suboxide structure are mainly discussed: random mixture^[63] and random bonding.^[64] The former model suggests the segregation of Si in silica separated by the interfacial boundary and the latter model suggests a continuous random network of tetrahedral units of SiSi_yO_{4-y} where $\gamma = 0$ to 4. The complexity of the network makes the material electronically interesting and, of course, span a-Si to amorphous silica.

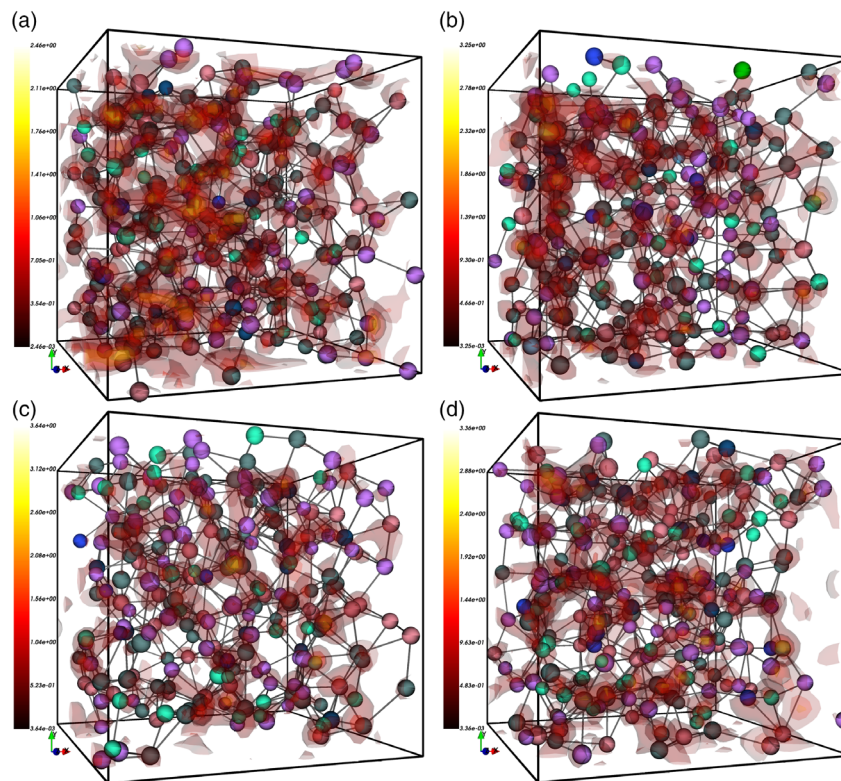


Figure 10. I-Si: SPC (ζ) projected on grids as a heat map plot (labeled by colorbars on left of each subplots) for configurations at intervals of 1.2 ps. a–d) The SPC plot at simulation time 1.95, 3.15, 4.35, and 5.55 ps, respectively. Atoms color represents Si with different coordination environment and we adopt the same convention as in Figure 9. The cutoff distance of 3.10 Å is used to define the coordination. Note the spatial fluctuation in the heat maps over these snapshots.

If one imagines starting in a-SiO₂, a superb insulator, one can imagine a process of randomly depleting O atoms from the network. If x is close to 2, O-vacancies will be widely separated with little conduction. As O depletion proceeds, more and more hopping will accrue and the conduction paths will be determined by the locations and electronic structure associated with the O-vacancy subnetwork. The electrical conductivity therefore has a stochastic character depending on the existence and details of a hopping pathway involving the vacancies. For small enough systems, the stochasticity in conduction path affects the observed DC conductivity, and makes an excellent PUF, as we report elsewhere.^[65]

In this article, we look very briefly at an AC version of this, and show that light absorption is very sensitive to wavelength, and in particular, show that different vacancy subnetworks contribute to the absorption. This suggests that an “optical PUF” might be possible for the silicon suboxide materials. We limit the discussion to a qualitative indication of how different parts of the network participate for two different wavelengths, and we note for completeness that to really carry out such calculations realistically better excited states should be computed with more intricate methods.

In this subsection, we discuss light absorption in a-SiO_{1.3} at two frequencies. To enable this, we calculated the space-projected conductivity on $40 \times 40 \times 40$ grids ($h = 0.39$ Å) for two different wavelengths with $\lambda = 2000$ nm and $\lambda = 1600$ nm. The SPC for both cases are shown in Figure 11. It is of interest that the

absorbing parts of the models are *qualitatively* different, and more to the point, the computation predicts *which* parts of the matrix will absorb light of a specified wavelength. The isosurface plots in Figure 11 show that the absorption meanders along adjacent O-vacancy sites in the network because different frequencies pick out different paths φ in the network. As such, changing the frequency and changing the path make it likely that external observables, such as absorption, will also change, making the system potentially attractive for PUF applications.

6.5. FCC Aluminum

So far we have discussed conduction in noncrystalline semiconductor materials. In this subsection, we consider FCC aluminum (c-Al), a metal, with a focus on the spectral properties of the conduction matrix Γ . $\Gamma(x, x')$ for the 500 atoms Al cell was obtained on a $42 \times 42 \times 42$ grids ($h = 0.48$ Å) so that $\dim(\Gamma) = 74\,088$. Γ was exactly diagonalized to obtain eigenvalues (Λ_μ) and the eigenvectors (χ_μ).

Figure 12 shows the DOS of the conduction eigenvalues and the extent of the localization of the conjugate eigenvectors (\mathcal{L}). The DOS in Figure 12 shows that a majority of the eigenvalues lie near $\Lambda = 0$. This is clear from the inset that shows the evolution of the conduction eigenvalues in increasing magnitude where only the last $\approx 24\,088$ among 74 088 eigenvalues have magnitude

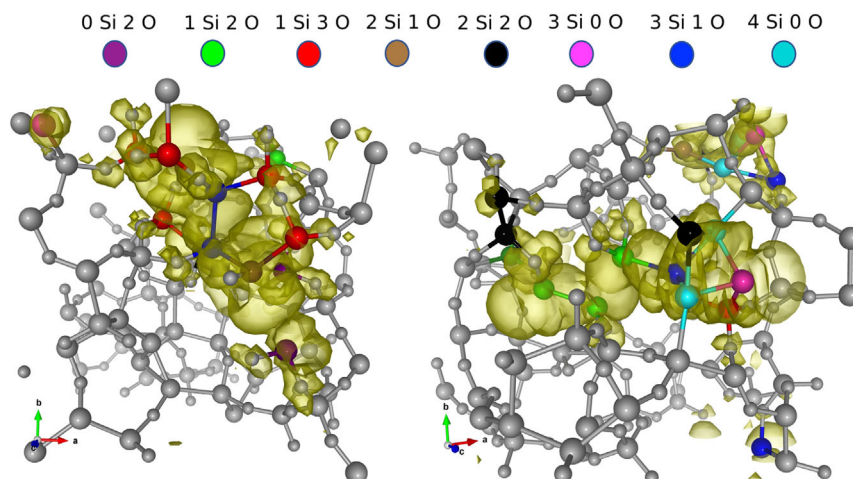


Figure 11. a-SiO_{1.3}: SPC (ζ) projected on grids as isosurface (yellow blobs) plots. Left and right plots correspond to $\hbar\omega = 0.62$ and 0.76 eV, respectively. Multicolored spheres refer to Si atoms within the conduction-active region having different coordination environment shown as legends at the top of the figure. Top 3.7% SPC values are included in both plots. The gray colored spheres represent Si and O atoms that lie outside the conduction active region for the given cutoff. The small size spheres represent O atoms.

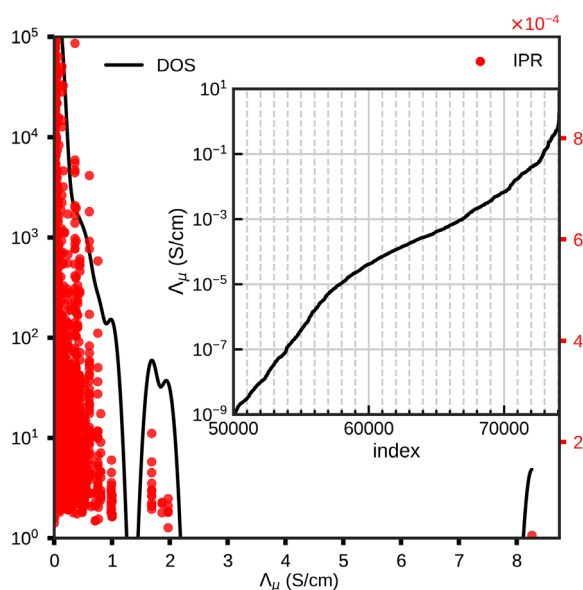


Figure 12. c-Al: Logarithmic spectral DOS of Γ matrix. The left scale corresponds to DOS of the eigenvalues displayed in a log scale (solid black line) and the right scale corresponds to the extent of localization measured as IPR (\mathcal{I}) (red circles). The inset shows the magnitude of conduction eigenvalues in ascending order.

greater than 10^{-9} S cm⁻¹. Even in a metal, most eigenvalues of Γ are effectively zero.

In contrast with our previous examples, the spectrum shows the presence of an extended tail in the DOS that reveals a signature of metallic conduction in Al. This is supported by the inset plot where the eigenvalue increases in a linear fashion at different regimes. The inset also provides a tentative picture of the transition from an insulating to conducting spectral character near the high- Λ end of the spectrum between indices

$\approx 60\,000$ – $67\,000$. Beyond index $\approx 67\,000$, we observe that the density of eigenvalues increases in a more quadratic manner. The presence of the tail in the DOS requires many eigenvectors to be considered to obtain the conduction path in Al (which is, of course, fully delocalized through the cell). A small spectral gap appears near $\Lambda_\mu = 1.3$ S cm⁻¹ from a physical origin that we have not yet determined. The other difference we find is the localization of the conduction eigenvectors where the modes are more extended for Al compared with what was observed in a-Si and the low-density a-C model.

Figure 13 shows the conduction eigenvalues (Λ_μ) plotted against IPR (\mathcal{I}). We see that for small IPR, there exists a fairly clear inverse relation between eigenvalues and the IPR. We also see Λ_μ near zero for low IPR. The eigenvectors corresponding to such eigenvalues can involve many sites, but always without forming any connected pattern and therefore corresponds to the nonconductive structures.

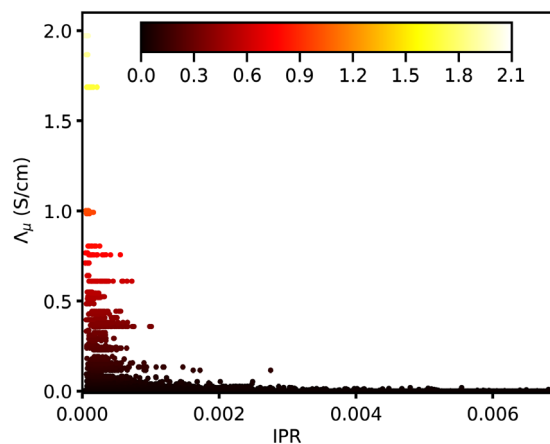


Figure 13. c-Al: The correlations of the eigenvalues with IPR (\mathcal{I}) shown by the scattered plots as heatmap. The colorbar at the central top of the figure refers to the magnitude of eigenvalues.

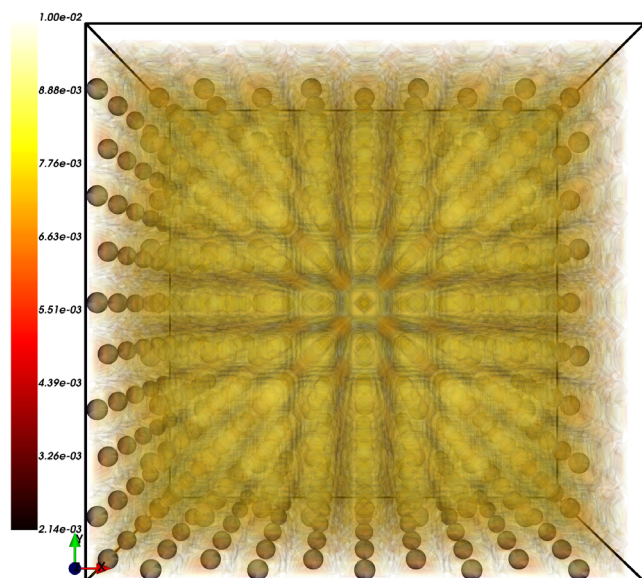


Figure 14. c-Al: Conductivity projected on grids weighted by the eigenvalues from all eigenvectors as a heat map plot (labeled by colorbars on the left) scaled with maximum value. The spheres represent Al atoms.

To visualize the conduction (really to see how a metallic conducting continuum emerges from this theory), we projected the conductivity from all the eigenvectors weighted by their eigenvalues and this is shown as a heat map plot in **Figure 14**. The electrons in c-Al are highly delocalized, as a result the projected values are essentially the same throughout the cell as shown in **Figure 14**. This is, of course, quite different from the semiconductors like a-Si and low-density a-C where only some parts of the material serve as the conduction-active sites in the network that we discussed in the earlier subsection.

The other interesting property we find in the spectrum of the DOS in c-Al (refer to **Figure 12**) is the presence of the degenerate eigenvalues toward the large Λ end of the spectrum. This is absent in the spectrum of a-Si and the low-density a-C. The degeneracy is surely a manifestation of the degeneracy present in the electronic levels, accruing in turn from the crystalline

symmetry (Only the $k=0$ point is used to sample the Brillouin zone, perhaps reasonable for a 500 atoms cell for this application, though in general this would be a doubtful approximation for a metal with its Fermi surface.). To visualize the conduction channel formed by the family of such degenerate eigenvalues, we projected the eigenvectors onto real space grids. **Figure 15** shows the projection of eigenvectors for one of such family of the degenerate eigenvalues as a heatmap plot. The left plot shows that the eigenvectors split into four conduction channels within the supercell. The channels possess an inversion symmetry at the center of the supercell. The middle and the right heat maps correspond to the eigenvectors for other two eigenvalues in the family which direct along different directions, namely, along x and y direction.

7. Conclusions

We presented a method to compute a conductivity projected onto real space grids, and we analyzed the spectral properties of the conduction matrix for a representative systems. For low-density a-C, we find that the sp^2 and sp configurations form active conduction sites. The conduction path is formed between the sp chains and the pentagonal or hexagonal graphene rings in the network. For a-Si, we find SPC is distributed at nearby atomic sites at different parts in the network, suggesting the possibility of hopping mechanisms for the electronic conduction. For a-Si, we find that the extreme eigenvectors pick atomic sites with different topology, involving tail states and strain defects for this fourfold WWW model. We also studied fluctuations in the energy levels in l-Si and provided the conduction path for few configurations. We showed that the fourfold, fivefold, sixfold, and sevenfold Si atoms form the conduction sites in the l-Si. We showed that diagonalization of $\Gamma(x, x')$ provides essential information about the nature of the conduction eigenmodes in different materials and helpfully categorizes the “paths” according to eigenvalue. From the spectrum of DOS of conduction eigenvalues, we always find a very large weight near $\Lambda = 0$. So, for materials like a-Si and a-C, only a few eigenvectors are sufficient to define the conduction path. For c-Al, we find that despite a significant accumulation of eigenvalues near $\Lambda = 0$,

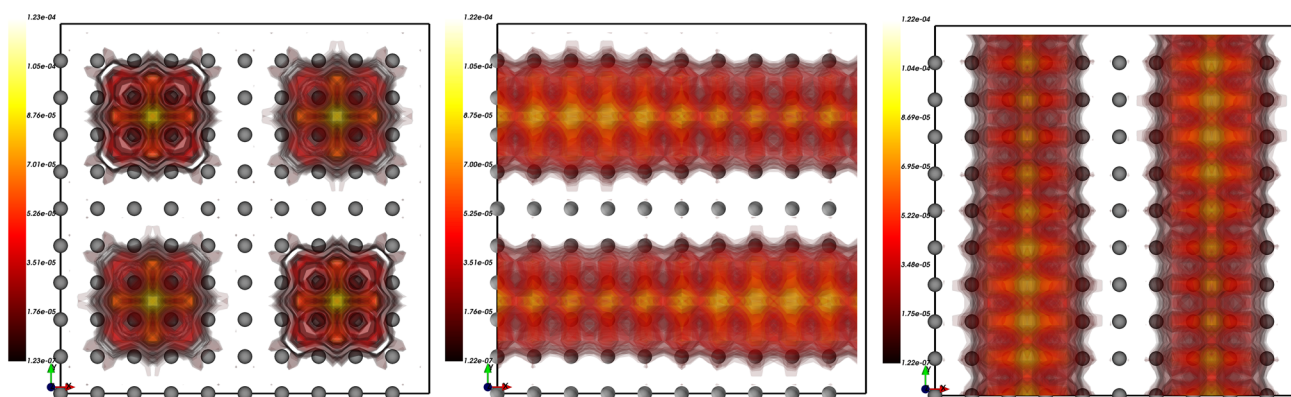


Figure 15. c-Al: Isosurface plots for eigenvectors corresponding to the degenerate eigenvalues ($\Lambda_\mu = 1.0013 \text{ S cm}^{-1}$). The isosurface plot displayed as a heat map (labeled by the colorbars on left of each subplots) includes the values within 0.001 times the maximum value on the grids. Al atoms are represented by gray spheres in each plot.

there is a spectral tail in the DOS and the channels corresponding to these states are extended. So, for metals, many eigenvectors are necessary to describe the conduction. We also observe a degeneracy in the conduction eigenvalues in the DOS of c-Al absent in the amorphous systems. We analyzed eigenvectors for one such degenerate eigenvalue near the extreme side of the spectrum and showed that these eigenvectors form a well-defined conduction channel. We also provided an example of a silicon suboxide ($\alpha\text{-SiO}_{1.3}$), where we projected the SPC for ($\omega > 0$) and showed that the O-vacancy sites form the major sites of conduction in such material.

In our previous works, we studied conduction mechanisms in few resistive memory materials, namely, $\alpha\text{-Al}_2\text{O}_3:\text{Cu}$ ^[7,28] and $\alpha\text{-Ta}_2\text{O}_5:\text{Cu}$ ^[29]. In both cases, we find that the Cu atoms segregate and form a cluster-like structure in the highly ionic host. We obtained the SPC and showed that these clustered Cu atoms form major conduction-active sites in these materials, indicating the metallic conduction in such systems. In $\alpha\text{-Ta}_2\text{O}_5:\text{Cu}$, we also find that the under-coordinated Ta atoms (O-vacancies) that are neighbors to Cu atoms are other sites of conduction. In $\alpha\text{-Al}_2\text{O}_3:\text{Cu}$, we showed that the connectivity of the Cu atoms in the network is vital to enhance the conductivity in the material. We also showed that in such a mixed (insulating/conducting) system, only a few eigenvectors of Γ are required to characterize conduction in the system.

No article is complete without *caveats*. It is not easy to extract quantitative conductivities for amorphous solids. Electron-phonon couplings are not included in static lattice computations and such temperature dependence is hardly a small effect. This is probably one reason why there are more computations of electrical conductivity in liquid metals, where dynamical effects (changes in electronic structure and therefore conduction due to atomic motion) are treated with Born–Oppenheimer dynamics. Also, in principle, methods producing accurate excited states perhaps using hybrid functionals should be used, and would doubtless make a significant difference in the numerical value of the conductivity. However, we emphasize that the qualitative character of the SPC is far less sensitive to these effects than the numerical value of the conductivity, and the method offers a fairly robust picture of conduction activity in complex materials.

Acknowledgements

The authors thank the National Science Foundation (NSF) for support under DMR award 1507670, and Extreme Science and Engineering Discovery Environment (XSEDE), supported by NSF grant number ACI-1548562 for providing computational resources under allocations DMR-190008P. The authors thank Prof. M. N. Kozicki of Arizona State University, who catalyzed and collaborated with us on this research, Mr. Greg Rosen of Ohio University, and Dr. Felix Mocuano of the University of Cambridge for helpful comments concerning conduction processes in $\alpha\text{-C}$. The authors thank Dr. Bishal Bhattarai for providing the model of low-density $\alpha\text{-C}$.

Conflict of Interest

The authors declare no conflict of interest.

Keywords

conduction eigenvectors, electronic conductivity, Kubo–Greenwood formula

Received: August 8, 2020

Revised: November 12, 2020

Published online:

- [1] P. B. Allen, in *Conceptual Foundations of Materials: A Standard Model for Ground- and Excited-State Properties* (Eds: S. G. Louie, M. L. Cohen), Elsevier, Amsterdam **2006**, Ch. 6.
- [2] J. M. Ziman, *Principles of the Theory of Solids*, 2 ed., Cambridge Press, Cambridge, **1972**.
- [3] R. Kubo, *J. Phys. Soc. Jpn.* **1957**, *12*, 570.
- [4] D. A. Greenwood, *Proc. Phys. Soc.* **1958**, *71*, 585.
- [5] R. Kubo, M. Toda, N. Hashitsume, N. Saito, *Statistical Physics. II: Nonequilibrium Statistical Mechanics*, Springer, Berlin **1985**.
- [6] A. Einstein, *Ann. Phys. (Leipzig)* **1905**, *322*, 549.
- [7] K. Prasai, K. N. Subedi, K. Ferris, P. Biswas, D. A. Drabold, *Phys. Status Solidi RRL* **2018**, *12*, 1800238.
- [8] N. F. Mott, E. A. Davis, *Electronic Processes in Non-crystalline Materials*, 2nd ed. (Eds.: N. F. Mott, E. A. Davis), Clarendon Press/Oxford University Press, Oxford/New York **1979**.
- [9] L. L. Moseley, T. Lukes, *Am. J. Phys.* **1978**, *46*, 676.
- [10] M. Zhang, D. A. Drabold, *J. Phys.: Condens. Matter* **2011**, *23*, 085801.
- [11] M.-L. Zhang, D. A. Drabold, *Phys. Rev. B* **2010**, *81*, 085210.
- [12] M. Zhang, D. A. Drabold, *Phys. Rev. E* **2011**, *83*, 012103.
- [13] G. Galli, R. M. Martin, R. Car, M. Parrinello, *Phys. Rev. B* **1990**, *42*, 7470.
- [14] A. N. Sobolev, A. A. Mirzoev, *J. Phys.: Conf. Ser.* **2008**, *98*, 062015.
- [15] S. K. Bose, O. Jepsen, O. K. Andersen, *Phys. Rev. B* **1993**, *48*, 4265.
- [16] M. P. Desjarlais, J. D. Kress, L. A. Collins, *Phys. Rev. E* **2002**, *66*, 025401.
- [17] J. Dong, D. A. Drabold, *Phys. Rev. Lett.* **1998**, *80*, 1928.
- [18] C. Landauro, H. Solbrig, *Mater. Sci. Eng., A* **2000**, *294–296*, 600.
- [19] B. D. Hoi, M. Yarmohammadi, *J. Magn. Magn. Mater.* **2018**, *451*, 57.
- [20] D. Drabold, *J. Non-Cryst. Solids* **2000**, *266–269*, 211.
- [21] R. Atta-Fynn, P. Biswas, D. A. Drabold, *Phys. Rev. B* **2004**, *69*, 245204.
- [22] K. Prasai, P. Biswas, D. A. Drabold, *Semicond. Sci. Technol.* **2016**, *31*, 073002.
- [23] D. A. Drabold, P. A. Fedders, *Phys. Rev. B* **1999**, *60*, R721.
- [24] T. A. Abtew, M. Zhang, D. A. Drabold, *Phys. Rev. B* **2007**, *76*, 045212.
- [25] L. Calderin, V. Karasiev, S. Trickey, *Comput. Phys. Commun.* **2017**, *221*, 118.
- [26] K. Prasai, G. Chen, D. A. Drabold, *Phys. Rev. Materials* **2017**, *1*, 015603.
- [27] K. N. Subedi, K. Prasai, D. A. Drabold, *Modelling of Glasses: Electronic conduction mechanisms in $\text{GeSe}_3\text{:Ag}$ and $\text{Al}_2\text{O}_3\text{:Cu}$* , World Scientific Publishing, Singapore **2020**.
- [28] K. N. Subedi, K. Prasai, M. N. Kozicki, D. A. Drabold, *Phys. Rev. Materials* **2019**, *3*, 065605.
- [29] R. Thapa, B. Bhattarai, M. N. Kozicki, K. N. Subedi, D. A. Drabold, *Phys. Rev. Mater.* **2020**, *4*, 064603.
- [30] C. E. Parman, N. E. Israeloff, J. Kakalios, *Phys. Rev. B* **1993**, *47*, 12578.
- [31] B. Xiao, T. Gu, T. Tada, S. Watanabe, *J. Appl. Phys.* **2014**, *115*, 034503.
- [32] R. B. S. Oakeshott, A. MacKinnon, *J. Phys.: Condens. Matter* **1994**, *6*, 1513.
- [33] H. U. Baranger, A. D. Stone, *Phys. Rev. B* **1989**, *40*, 8169.
- [34] M. Paulsson, M. Brandbyge, *Phys. Rev. B* **2007**, *76*, 115117.
- [35] C. Lanczos, *Applied Analysis*, Prentice-Hall, Englewood Cliffs, NJ **1956**.
- [36] D. A. Drabold, O. F. Sankey, *Phys. Rev. Lett.* **1993**, *70*, 3631.
- [37] G. Kresse, J. Hafner, *Phys. Rev. B* **1993**, *47*, 558.
- [38] J. P. Perdew, K. Burke, M. Ernzerhof, *Phys. Rev. Lett.* **1996**, *77*, 3865.

- [39] B. Bhattacharai, D. A. Drabold, *Carbon* **2017**, *115*, 532.
- [40] B. R. Djordjević, M. F. Thorpe, F. Wooten, *Phys. Rev. B* **1995**, *52*, 5685.
- [41] A. Barranco, F. Yubero, J. P. Espinós, P. Groening, A. R. González-Elipe, *J. Appl. Phys.* **2005**, *97*, 113714.
- [42] D. A. Drabold, *Eur. Phys. J. B* **2009**, *68*, 1.
- [43] R. M. Feenstra, M. Widom, www.andrew.cmu.edu/user/feenstra/wavetrans, **2012**.
- [44] D. S. da Silva, A. D. S. Cortes, M. H. Oliveira, E. F. Motta, G. A. Viana, P. R. Mei, F. C. Marques, *J. Appl. Phys.* **2011**, *110*, 043510.
- [45] A. Grill, *Diamond Rel. Mater.* **1999**, *8*, 428.
- [46] K. Park, E. Chin, *Polym. Degrad. Stab.* **2000**, *68*, 93.
- [47] P. L. McEuen, *Nature* **1998**, *393* 585.
- [48] R. J. Nicholas, A. Mainwood, L. Eaves, *Philos. Trans. R. Soc., A* **2008**, *366*, 189.
- [49] K. S. Novoselov, A. K. Geim, S. V. Morozov, D. Jiang, Y. Zhang, S. V. Dubonos, I. V. Grigorieva, A. A. Firsov, *Science* **2004**, *306*, 666.
- [50] A. K. Geim, K. S. Novoselov, *Nat. Mater.* **2007**, *6*, 183.
- [51] S. T. C. Konigsmark, L. K. Hwang, D. Chen, M. D. F. Wong, In *2014 19th Asia and South Pacific Design Automation Conf. (ASP-DAC)*, Singapore **2014**, pp. 73–78.
- [52] S. A. Wring, J. P. Hart, *Analyst* **1992**, *117*, 1215.
- [53] B. Bhattacharai, P. Biswas, R. Atta-Fynn, D. Drabold, *Phys. Chem. Chem. Phys.* **2018**, *20*, 19546.
- [54] R. A. Street, *Hydrogenated Amorphous Silicon*, Cambridge Solid State Science Series, Cambridge University Press, Cambridge **1991**.
- [55] P. A. Fedders, D. A. Drabold, S. Nakhmanson, *Phys. Rev. B* **1998**, *58*, 15624.
- [56] Y. Pan, F. Inam, M. Zhang, D. A. Drabold, *Phys. Rev. Lett.* **2008**, *100*, 206403.
- [57] T. Abtew, M. Zhang, Y. Pan, D. Drabold, *J. Non-Cryst. Solids* **2008**, *354*, 2909.
- [58] F. Inam, J. P. Lewis, D. A. Drabold, *Phys. Status Solidi A* **2010**, *207*, 599.
- [59] P. A. Fedders, D. A. Drabold, S. Klemm, *Phys. Rev. B* **1992**, *45*, 4048.
- [60] T. H. Kim, G. W. Lee, B. Sieve, A. K. Gangopadhyay, R. W. Hyers, T. J. Rathz, J. R. Rogers, D. S. Robinson, K. F. Kelton, A. I. Goldman, *Phys. Rev. Lett.* **2005**, *95*, 085501.
- [61] J. T. Okada, P. H.-L. Sit, Y. Watanabe, Y. J. Wang, B. Barbiellini, T. Ishikawa, M. Itou, Y. Sakurai, A. Bansil, R. Ishikawa, M. Hamaishi, T. Masaki, P.-F. Paradis, K. Kimura, T. Ishikawa, S. Nanao, *Phys. Rev. Lett.* **2012**, *108*, 067402.
- [62] C. Mesaritakis, M. Akriotou, A. Kapsalis, E. Grivas, C. Chaintoutis, T. Nikas, D. Syvridis, *Sci. Rep.* **2018**, *8*, 9653.
- [63] G. W. Brady, *J. Phys. Chem.* **1959**, *63*, 1119.
- [64] H. R. Philipp, *J. Non-Cryst. Solids* **1972**, *8–10*, 627.
- [65] K. N. Subedi, M. N. Kozicki, D. A. Drabold, *Conduction Mechanisms in Silicon Suboxides*, unpublished.